ACS APPLIED MATERIALS & INTERFACES

Research Article

www.acsami.org

Nanodiamond-Based Thermal Fluids

Jose Jaime Taha-Tijerina,*,[†] Tharangattu Narayanan Narayanan,[‡] Chandra Sekhar Tiwary,[†,§] Karen Lozano,[⊥] Mircea Chipara,[#] and Pulickel M. Ajayan[†]

[†]Department of Materials Science and NanoEngineering, Rice University, Houston, Texas 77005, United States

[‡]Council of Scientific and Industrial Research−Central Electrochemical Research Institute (CSIR-CECRI), Karaikudi 630006, India

[§]Materials Engineering, Indian Institute of Science, Bangalore 560012, Karnataka, India

[⊥]Mechanical Engineering Department and [#]Department of Physics and Geology, The University of Texas Pan American, Edinburg, Texas 78539, United States

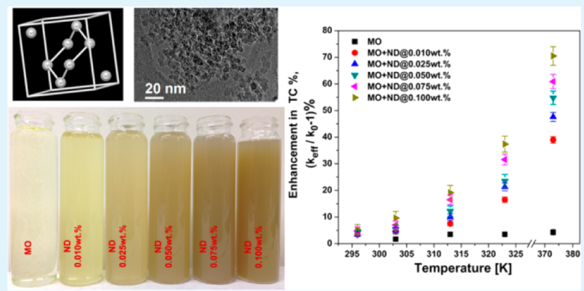

ABSTRACT: Dispersions of nanodiamond (average size ∼6 nm) within dielectric insulator mineral oil are reported for their enhanced thermal conductivity properties and potential applications in thermal management. Dynamic and kinematic viscosities—very important parameters in thermal management by nanofluids—are investigated. The dependence of the dynamic viscosity is well-described by the theoretical predictions of Einstein's model. The temperature dependence of the dynamic viscosity obeys an Arrhenius-like behavior, where the activation energy and the pre-exponential factor have an exponential dependence on the filler fraction of nanodiamonds. An enhancement in thermal conductivity up to 70% is reported for nanodiamond based thermal fluids. Additional electron microscopy, Raman spectroscopy and X-ray diffraction analysis support the experimental data and their interpretation.

KEYWORDS: *nanofluids, diamond, mechanical properties, thermal conductivity, viscosity*

1. INTRODUCTION

A revolution in the field of heat transfer fluids (HTFs) arose with the advent of nanofluids (NFs), a term introduced by Choi's research group in the late 90's at Argonne National Lab (ANL). Nanofluids consist of homogeneously suspended nanostructures (< 100 nm) within conventional fluids. These suspended ultrafine structures such as oxide, nitride, and carbide ceramics, metals, semiconductors, carbon nanotubes (CNTs), and composite materials with diverse shapes and sizes possess higher thermal conductivity than the conventional fluids.[1−5] Various studies on the type and morphology of the reinforcing nanostructures and of different base fluids, such as water, ethylene glycol (EG), and various types of oils, have been reported. However, the inherent limitation of conventional fluids is their relatively low thermal conductivity.[5−8] What these conventional fluids lack in thermal conductivity is compensated by their ability to flow; water for instance, is roughly three orders of magnitude less thermally conductive than copper or aluminum.[9,10]

HTFs loaded with various nanoparticles are affected by a wide variety of factors such as fluid stability, composition, viscosity, surface charge, Brownian motion, interfacial layering, agglomeration, interface and morphology of the dispersed particles, etc.[11−15] Optimization and high efficiency of components and devices have gained great importance because these factors play a paramount role in diverse fields such as heat transfer, component and tool wear, machining/metal-mechanic operations (stamping, drilling, etc.), medical therapy and diagnosis, biopharmaceuticals, air conditioning, fuel cells, high-voltage power transmission systems, solar cells, micro/nanoelectronic mechanical systems (MEMS/NEMS), and engine and nuclear reactor cooling, among others.[2−8,16]

One of the main advantages of nanofluids is that they can be engineered to optimally fulfill particular objectives, such as reduced friction and anti-wear properties, enhanced thermal conductivity, higher thermal energy storage capacity, a higher heat transfer coefficients, better temperature stabilization, and less pressure drop.[16,17] Moreover, nanofluids are promising for practical application that eliminates or reduce clogging or sedimentation.

Nanodiamond (ND) inherits most of the outstanding material properties of bulk diamond and delivers them at the nanoscale.[18−23] Some of these properties are superior hardness, lubricity, high thermal conductivity and electrical resistivity, chemical stability, and biocompatibility among several others. This research exploits the high thermal conductivity of ND, which for single crystal diamond (IIa type) it is as high as typically ranges between 900 and 2300 W/(m K) at room temperature.[24] The thermal conductivity strongly depends on the crystallinity and on the concentration/nature of impurities.[25] The characteristic value for diamond single crystal made of 99% ^{12}C, at 104 K was measured to be ∼40 000 W/(m

Received: December 4, 2013
Accepted: March 21, 2014
Published: March 21, 2014

K),[24,26] which is the highest thermal conductivity measured above liquid nitrogen temperature and it is 100 times greater than the thermal conductivity of copper (~400 W/(m K)).[10]

Various types of nanofillers have been used to prepare nanofluids for different applications. For instance, a 70% increase in thermal conductivity of EG was obtained by adding 1.0 vol % ultradispersed ND structures according to Kang et al.[27] Nanodiamonds (< 10 nm) dispersed in EG (with addition of poly(glycidol) polymer) and mineral oil (with addition of oleic acid as surfactant) were studied by Branson et al.[22] It was observed that addition of 0.88 vol % NDs within EG enhanced the effective thermal conductivity by about 12%. In MO, for instance, an enhancement in thermal conductivity of ~6% and ~11% was achieved by NDs loading of 1.0 and 1.9 vol %, respectively. According to Branson et al.,[21] the differences between these improvements could be explained by the divergence in thermal boundary resistance at nanoparticle/surfactant interfaces.[22]

Nanofluids prepared with allotropes of carbon (CNTs, diamond, graphene oxide, etc.) and oxide-based nanofluids usually contain more than 0.50−1.0 wt % filler fraction. Up to 10−12 wt % filler fraction of nanofillers have been incorporated to base fluids in order increase the thermal conductivity (typically by at least 15%).[18,19,22,28−31] However, such concentrations of nanofillers increase the suspensions viscosity, as well as nanofluids costs. This adversely affects the fluidity and jeopardizes the nanofluid stability and the thermal management goals.

This research focuses on the viscosity and thermal conductivity characterization of nanofluids containing very low filler fraction of nanodiamonds (< 0.10 wt %) within mineral oil, without the usage of any surfactants.

2. MATERIALS AND METHODS

2.1. Materials. Standard electrically insulating mineral oil (MO) is chosen as a base fluid. MO is commonly used for its electrical insulating capabilities and fluid features in electrical motors and high-voltage power transmission systems. The main specifications of the MO utilized in this work are shown in Table 1. Nanodiamonds (NDs) in a powder form have been obtained from Nanostructured & Amorphous Materials, Inc. The nanodiamonds have a density of 3.05−3.30 g/cm^3.

2.2. Nanofluid Preparation. Nanodiamonds particles are considered ideal fillers because of their low electrical conductivity and excellent thermal conductivity. Nanofluids were prepared by dispersing ND powder within MO at various filler fractions, in the range of 0.01−0.10 wt %. Glass vials of 33 mL were used to maintain the samples. The vials containing the dispersions were sonicated for several hours (~3−4 h.) in a water bath in order to keep the temperature constant (~300 K) and to homogenize the suspensions. Brownish solutions were obtained after sonication. These were stable for a few days (~2−3), until sedimentation of the nanodiamond particles occurred. To achieve high-quality dispersions and stabilization of nanostructures within base fluids, specialized processing techniques, such as surface functionalization (hydrogenation[32]) or use of surfactants, are usually required. In this research, no surfactants were used, because we aimed to investigate the thermal conductivity performance of nanodiamond-based fluid. The use of surfactants can adversely affect other properties, such as the effective thermal conductivity, because surfactants could introduce defects at the interfaces.[4] The free phonon/electron movement is affected by these defects, and hence a surfactant-free stable suspension can provide much better thermal conductivity. Research on the thermal and fluid features of ND/MO suspensions with no surfactants or additives is reported here.

Table 1. Main Specifications of the MO Utilized in This Research

property	test method	value and units	observations
density, 15 °C	ASTM D 1298	0.88−0.91 g/cm^3	
kinematic viscosity, 0 °C	ASTM D 445	76 mm^2/s	maximum value
kinematic viscosity, 40 °C	ASTM D 445	12 mm^2/s	maximum value
kinematic viscosity, 100 °C	ASTM D 445	3 mm^2/s	maximum value
flash point	ASTM D 92	145 °C	minimum value
pour point	ASTM D 97	−40 °C	
interfacial tension at 25 °C	ASTM D 971	40 mN/m	minimum value

Note: Information from supplier − Nynas Nytro 10XN.

Bath sonication (Branson ultrasonic homogenizer model 5510, 40 kHz) was used to homogeneously dispersing ND within MO (3−4 h). KD2 Pro (Decagon Device Inc.) was used for thermal conductivity measurements; a water bath to keep the samples at constant temperature was used during thermal conductivity measurements as well. Shear viscosity studies were conducted with a TA Instruments ARES rheometer. The ND particles were characterized using Raman spectroscopy, X-ray diffraction (XRD), and transmission electron microscopy (TEM). Raman spectroscopy measurements were carried out by a Renishaw MicroRaman spectrometer with a 633 nm diode laser. The XRD pattern of nanodiamonds was obtained using a Rigaku spectrometer with a Cu$_{K\alpha}$ source. TEM was performed using field-emission gun JEOL2100F.

3. RESULTS AND DISCUSSION

3. 1. Nanodiamond Characterization. Figure 1 shows the Raman spectrum of the as received nanodiamonds. The as recorded Raman spectrum of nanodiamonds is represented by gray circles, whereas the line reflects the best fit obtained by assuming that the Raman spectrum is a convolution of 6 lines, each characterized by a Breit−Wigner−Fano line shape.[33] The fitting revealed that all components of the Raman spectrum are Lorentzian, within 1% accuracy. The strongest line of the spectrum was noticed at 1320 cm^{-1} and it is in excellent agreement with the T_{2G} mode of diamond predicted

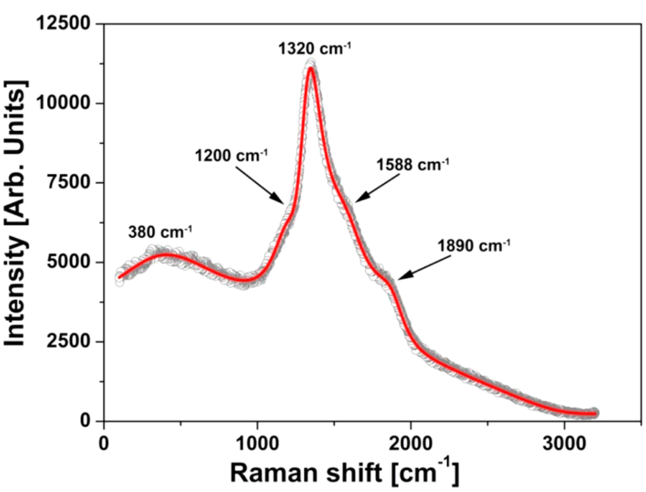

Figure 1. Micro-Raman spectrum of nanodiamond structures (gray circles) and best fit (thick line) obtained assuming that the spectrum is a convolution of 6 lines.

dx.doi.org/10.1021/am405575t | ACS Appl. Mater. Interfaces 2014, 6, 4778−4785

theoretically.[34] Mochalin et al. reported this peak at 1328 cm^{-1}.[17] Technically, this peak reflects the D band position in nanodiamonds.[35]

The Raman peak located at 380 cm^{-1} is associated with the breathing mode of nanodiamonds. Theoretical simulations[34] suggested for nanodiamonds with a size of about 1 nm the existence of a breathing mode below 400 cm^{-1}, supporting the proposed assignment. As expected, this peak is broad (half width of about 450 ± 10 cm^{-1}). The peak noticed at 1588 cm^{-1} is assigned to the G band and observed in the detonation soot.[17] The band located at about 3200 cm^{-1} can be an overtone (two phonon process of the G band located at 1587 cm^{-1}, sometimes labeled as 2G band.[33] The Raman spectrum is missing the fingerprints of oxidized nanodiamonds or residual C=O groups.[17]

The XRD pattern of dried ND powder (Figure 2) shows the most intense peak at 44.3°; corresponding to [111] reflections,

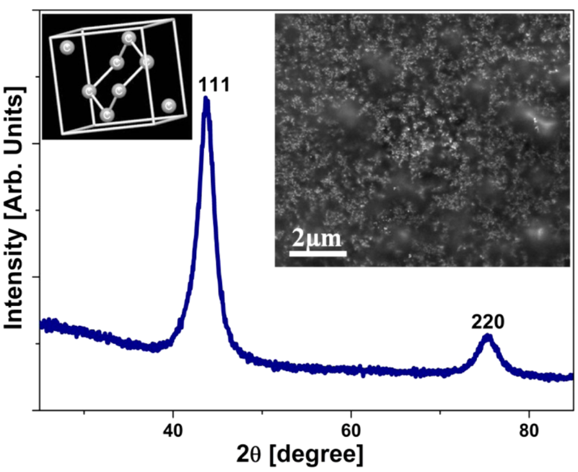

Figure 2. XRD pattern of nano-diamond powders marking the peaks. The XRD matches with cubic diamond crystal shown as inset. SEM images shows uniform size of diamond powder.

followed by another peak at 76.1°, assigned to 220 reflections. The above diffraction peaks corresponds to a lattice parameter of a = 0.3536 nm and angle α = 90 for a cubic diamond (space group $Fd\bar{3}m$ O2 (227)). The crystallite size calculated using Scherer formula[36] is found to be 6 ± 2 nm. The inset of Figure 2 shows uniform size distribution using a high-magnification SEM image covering large fraction of particles.

To observe the morphology, size, and conformation of nanodiamonds TEM microscopy has been performed. Figure 3a shows bright-field image consisting of several particles and selective area diffraction covering these particle. The Selected Area Diffraction (SEAD) shows three most intense peaks for [111], [220], and [311] reflections (Figure 3). The bright field image shows uniform size distribution of the nanodiamonds. In order to obtain the size distribution more than ten TEM images have been taken. Gatan digital micrograph software has been used to estimate the size of each particle that has been measured. The particle distribution plot shown in Figure 3b reveals particle size to be 4−8 nm which is consistent with XRD calculations and manufacturer's data. To observe the morphology and lattice structure, we have performed HRTEM imaging. Images c and d in Figure 3 show crystals with [100] and [111] orientation. The lattice orientation generated using diamond software for these two orientations are shown as inset. The FFT from these crystals are shown as inset on right top, which again confirms the orientation.

3.2. Viscosity. The improvement of the thermal conductivity by increasing the nanoparticles filler fraction is limited by the increase of viscosity, which will adversely affect the fluid properties. Hence, the search for new nanofillers, which can get high thermal conductivities at lower filler fractions, is important.[37]

In real devices or systems, the fluid flow is controlled by pumps and consequently viscosity plays a paramount role. As such, preliminary viscosity results were obtained for ND/MO nanofluids for various concentrations. The dependence of the kinematic viscosity on the weight fraction of nanodiamonds, at various temperatures is shown in Figure 3. It is observed that the enhancement of the kinematic viscosity due to the addition of ND filler is very small (<6% with 0.100 wt % at room temperature ~299 K), which is an added advantage of the low weight fractions. As expected, the viscosity of the nanosuspensions decreases significantly as the temperature is increased (see Figure 4).

Theoretical models developed for the viscosity of fluids are based on the use of dynamic viscosity and volume fractions. The relationship between the kinematic viscosity η_K and the dynamic viscosity η_D or briefly η is mediated by the density of the suspension ρ_S, according to:

$$\eta_D = \eta = \rho_S \eta_K \tag{1}$$

The density of the suspension ρ_S can be estimated within a first-order approximation by using the rule of phase

$$\rho_S \cong \rho_L(1 - \psi) + \rho_F \psi \tag{2}$$

Where ρ_L is the density of the fluid (MO density ~890 kg/m^3) and ρ_F is the density of the filler (NDs with a density of about 3100 kg/m^3). This expression is an acceptable approximation as the samples investigated were characterized by low filler fractions. The theoretical values of the density of the suspensions are collected in Table 2. Equation 2 neglects any interface between the nanoparticles and the fluid. However, the very low concentration of nanoparticles indicates that the corrections to the density of the dispersion due to the presence of an interface between nanoparticles and mineral oil are relatively small, making eq 2 an acceptable approximation.

To analyze the ND/MO nanofluids, it is necessary to convert the weight percent of ND into volume fractions. Taking into account the density of nanodiamonds and neglecting the formation of the interface, the conversion from the mass fraction ψ into the volume fraction φ, is given by

$$\psi = \frac{m_F}{m_L} = \frac{\varrho_F}{\varrho_L}\frac{V_F}{V_L} = \frac{\varrho_F}{\varrho_L}\phi \tag{3}$$

Overall, addition of nanoparticles within a fluid will be reflected by an increase in the viscosity. For a suspension of spherical particles within a fluid, the relationship between the viscosity of the suspension η_S and the viscosity of the fluid, η_F has been derived by Einstein in the so-called dilute regime[38,39]

$$\eta_S = \eta_F\left(1 + \frac{5}{2}\phi\right) \tag{4}$$

Where φ is the volume fraction of the filler within the fluid (i.e., the ratio between the volume of the filler and the volume of the solution). In the general case, for a dilute suspension of spherical particles, eq 4 can be expressed as:

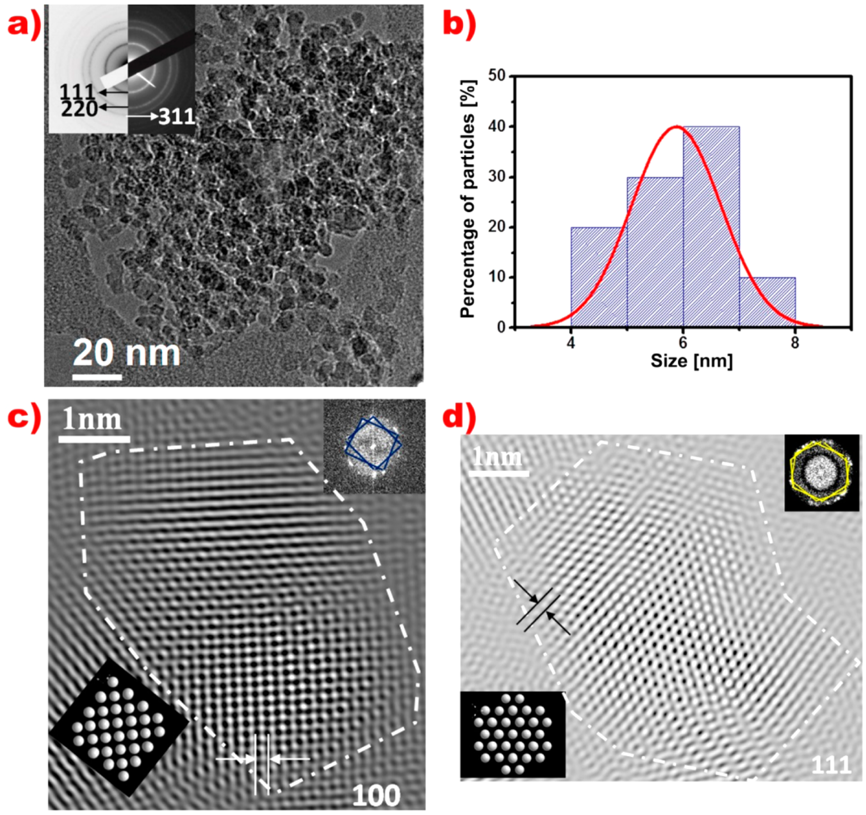

Figure 3. (a) Bright-field TEM micrograph of nanodiamond particles with SAD of these particles as inset showing diffraction planes. (b) Particles size distribution of the nanodiamonds. HRTEM image of the nanodiamond at two different crystal orientation (c) 100 and (d) 111 with inset showing lattice orientation (at bottom) and FFT at right top as inset.

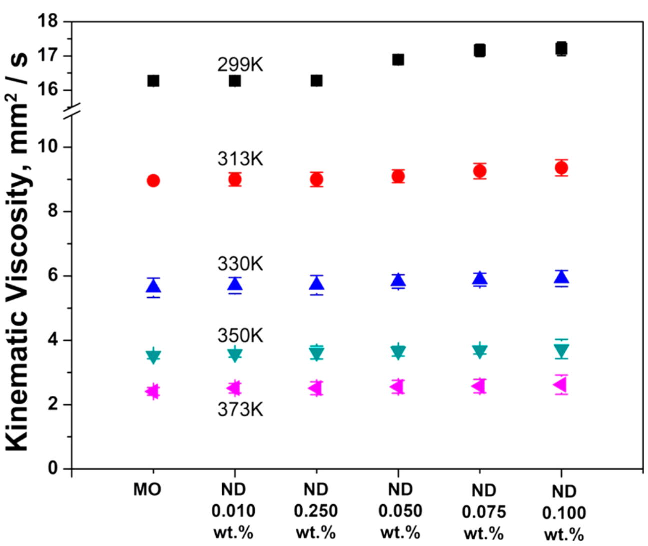

Figure 4. Temperature-dependent viscosity variation of ND/MO nanofluids at various filler fractions of nanodiamonds.

$$\eta_S = \eta_F(1 + C_1\phi) \quad (5)$$

Where C_1 is a constant. As can be observed from Figures 5 and 6, the addition of nanoparticles (NDs) to MO increases the viscosity of the oil, in agreement with eqs 4 and 5.

The best fit, at 25 °C (See Figure 5) is characterized by an acceptable correlation coefficient of 0.90 and corresponds to a fluid viscosity η_F =14.4 ± 0.1 Pas, and to a coefficient C_1 = 2.5 ± 0.3, in excellent agreement with eqs 4 and 5. Such an agreement is not unexpected as eq 4 has been developed theoretically for spherical fillers while the NDs have a cubic structure that approximates nicely a spherical morphology. In Figure 5, the thick line represents the best fit of experimental data, based on eq 5. The coefficient C_1 is identical to the value predicted by the Einstein theory for dilute spheres (see eq 4). The correlation coefficient is not 1.00 as expected for a perfect linear dependence. It seems that the main issues are coming for the viscosities estimated at very low filler fractions, where the experimental errors can be a little larger. However, more complex interactions between spheres or between the spheres and the fluid cannot be discarded.

Table 2. Estimated Values of the Density of the Suspensions and of the Volume Fraction from Measured Values of the Weight Fraction

	weight fraction (%)	density of suspension (kg/m^3)	volume fraction (%)
a	0	890	0
b	0.010	890.221	0.00287
c	0.025	890.5525	0.00718
d	0.050	891.105	0.01435
e	0.075	891.6575	0.02152
f	0.100	892.210	0.02870

An improved expression for the viscosity of suspensions has been suggested by several authors[38,39] and technically involves a quadratic correction to the eq 1

$$\eta_S = \eta_F(1 + C_1\phi + C_2\phi^2) \quad (6)$$

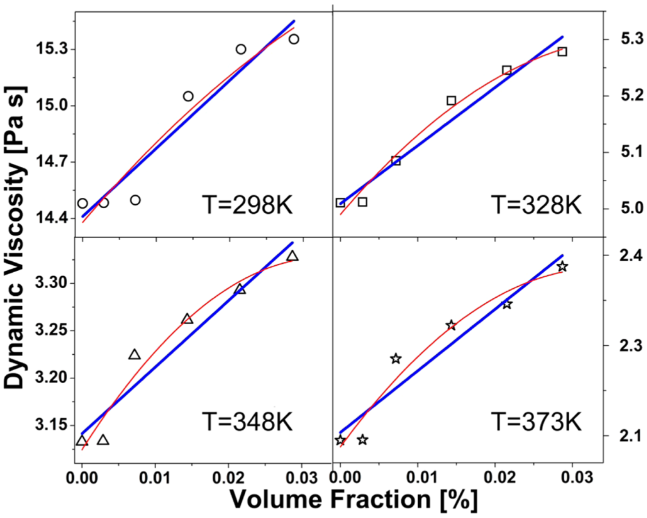

Figure 5. Dependence of the dynamic viscosity on the filler fraction of NDs at various temperatures. Empty geometrical shapes (circles, squares, etc.) represent the experimental data, thick lines the best fit obtained by using eq 5 and thin lines are associated with the best fit of experimental data obtained by using eq 6

Where C_1 and C_2 are constants. The best fit obtained using the eq 6 for the nanofluids at 25 °C corresponds to $\eta_F = 14.4 \pm 0.1$ Pa s, $C_1 = 3.2 \pm 1.5$, and $C_2 = -23.5 \pm 1.5$. The theoretical dependence defined by eq 6 is represented in Figure 5 by the thin (red) line. The correlation coefficient for this fit was slightly smaller (0.88) than the correlation coefficient for the linear dependence (see eq 5). The increased errors in the estimation of η_F and C_1, the smaller correlation coefficient and the (unexpected) negative value of the C_2 coefficient rules against taking into account the quadratic correction.

In conclusion, the viscosity of ND/MO nanofluids obeys the Einstein theory with some small deviations reflecting eventually interactions among nanoparticles (clusters) and enhanced errors at very small concentrations of nanofillers.

The temperature dependence of the viscosity of oil and of oil–nanodiamond suspensions was fitted by assuming and Arrhenius-like behavior

$$\eta_s = \eta_0 \exp\left(\frac{E_A}{K_B T}\right) \tag{7}$$

Where E_A is the activation energy for the viscosity, K_B is the Boltzmann constant, and T is the temperature (in K). As noticed from Figure 6, the temperature dependence of the viscosity obeys with a very good accuracy an Arrhenius like dependence. The red lines in Figure 6 represent the best fit of viscosity data, according to eq 7. The simulations of experimental data with an Arrhenius-like dependence indicated that both the activation energy and the pre-Arrhenius factor are affected by the volume fraction of the filler. For exemplification, the dependence of the activation energy E_A on the volume fraction of nanodiamonds is shown in Figure 7. Such behavior was expected because of the low concentration of nanodiamonds in oil.

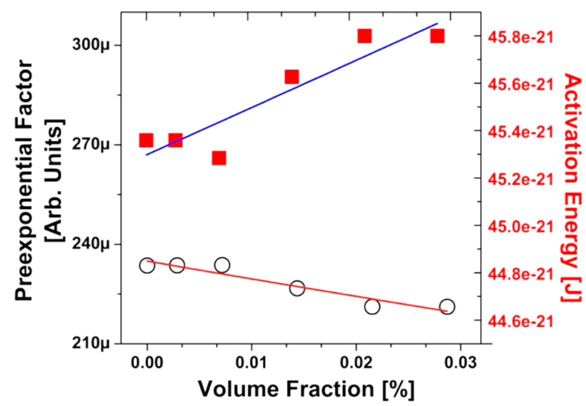

Figure 7. The dependence of the activation energy and pre-exponential factor on the volume fraction of NDs.

Figure 7 focuses on the dependence of the parameters of the Arrhenius like dependence (E_A and η_0) on the volume fraction of nanodiamonds. The dependence of the activation energy on the volume fraction of NDs (see the squares in Figure 7), indicates a monotonous increase of the activation energy as the volume fraction of NDs is increased. This reflects the effect of

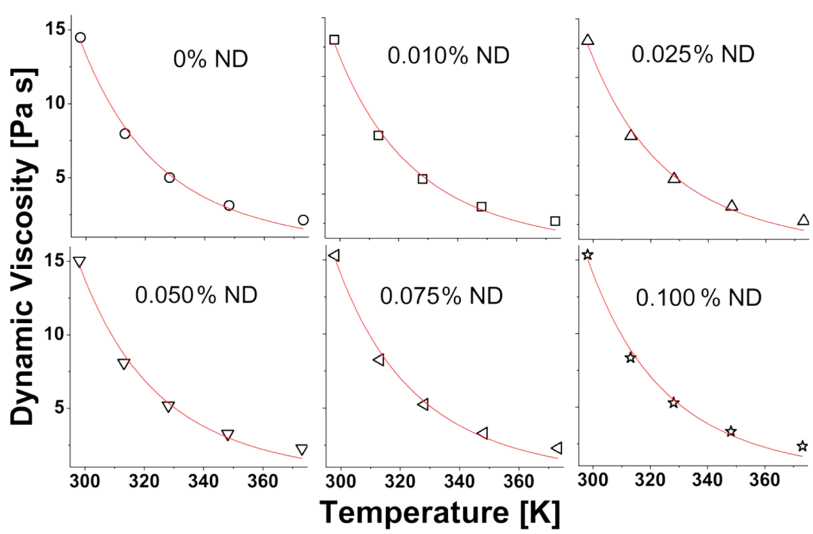

Figure 6. Dependence of the dynamic viscosity on temperature for suspensions containing various filler fractions of nanodiamonds. Experimental values are denoted by circles/squares/triangles/stars and theoretical fits are denoted by solid lines.

dx.doi.org/10.1021/am405575t | ACS Appl. Mater. Interfaces 2014, 6, 4778–4785

interactions among nanofillers, which is not negligible even in such diluted solutions. Tentatively, it was suggested that the dependence of the activation energy for the shear viscosity of MO/ND dispersions on ND volume fraction φ can be described by the expression

$$E_A = A\exp(B\phi) \quad (8)$$

Where A and B are constants. The best fit, represented in Figure 7 by a continuous line was obtained for $A = 4.530 \times 10^{-20} \pm 0.06 \times 10^{-20}$ J and B = 0.42 ± 0.08, with a very good correlation coefficient of 0.995.

The pre-exponential factor η_0, (represented in Figure 7 by open circles) shows a weak decrease as the concentration of nanofillers is increased reflecting the decrease of the average time between collisions as the concentration of ND is increased. The pre-exponential factor η_0 was assumed to exhibit an analogous dependence on the volume fraction of the nanofiller

$$\eta_0 = C\exp(D\phi) \quad (9)$$

Where C and D are constants. For the pre-exponential factor (see eq 9), the best fit was achieved for $C = 2.35 \times 10^{-4} \pm 0.02 \times 10^{-4}$ Pa s, $D = -2.3 \pm 0.1$, and a correlation coefficient of 0.98. It is noticed that in this case D is negative. To conclude, the overall dependence of the shear viscosity of these dispersions on temperature and on the volume fraction of ND is well described by the equation

$$\eta_s = \eta_0^* \exp\left(\frac{E_A^* \exp(B\phi)}{K_B T} - |D|\phi\right) \quad (10)$$

Where $\eta_0^* = \eta_0 C$ and $E_A^* = E_A A$.

The dependence of the shear stress on the shear strain rate is a straight line passing through origin. The same dependence was recorded for all solutions investigated (Figure 8 exemplifies

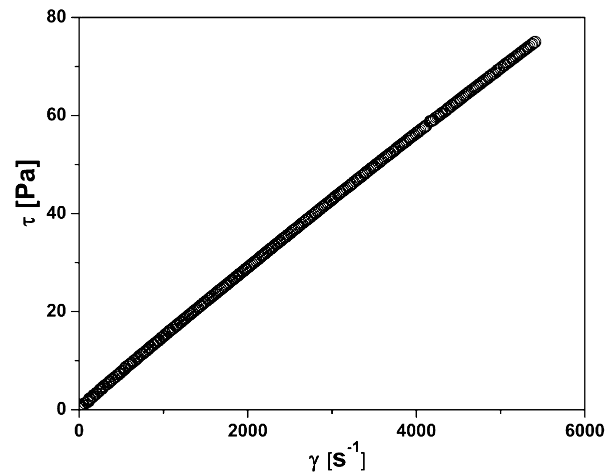

Figure 8. Dependence of the shear stress on the shear strain rate for MO. The symbol size is an estimation of the experimental error.

this behavior for the pure MO). This is an expected outcome, taking into account that this study was focused on dilute ND/MO solutions. To conclude, all solutions showed a linear viscoelastic behavior within the experimental errors.

3.2. Thermal Conductivity.

Thermal conductivity measurements at various filler fractions of nanodiamond were carried out following the transient hot-wire (THW) technique using a KS-1 probe (Decagon Device Inc., model KD2 Pro). The instrument uses a 1.3 mm diameter by 60 mm long stainless steel probe that is completely immersed in the nanofluid to obtain the effective thermal conductivity (k_{eff}) of the samples. This probe has been calibrated using a standard fluid, glycerol, and the conductivity value is verified up to 3 decimal points. Temperature-dependent measurements were done using a thermal bath, and samples were thermally equilibrated before each measurement. The measured values are compared with the base fluid (MO) thermal conductivity (k_0). Higher volumes (0.01wt %, 100 mL and ~250 mL) of fluids are also subjected to the thermal conductivity measurements using the same method, and it was found that their thermal conductivity values are within the error limit as that we obtained for 33 mL 0.01 wt % nanofluid.

Figure 9 shows the effect of temperature and filler fraction of ND/MO nanofluids. The thermal conductivity of MO (at room

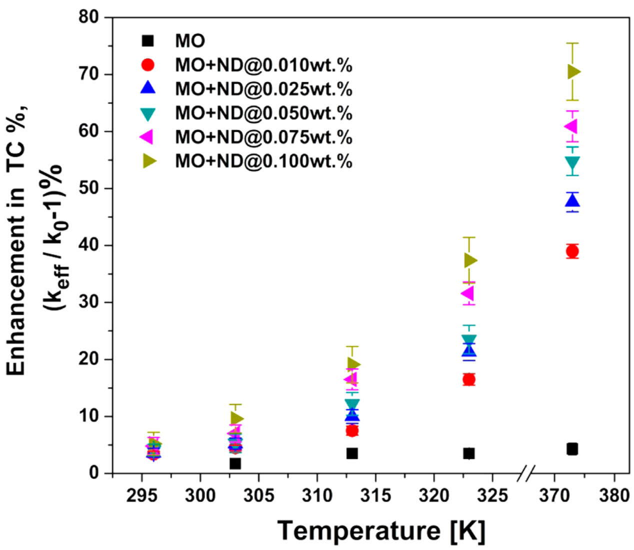

Figure 9. Temperature-dependent effective thermal conductivity enhancement of various nanofluids.

temperature, thermal conductivity of MO is ~0.115 W/m K, agreeing well with standard values reported) did not show any temperature dependence, as previously reported.[1] Moreover, an enhancement in thermal conductivity was observed at all elevated temperatures for all nanofluids, indicating the contribution of Brownian motion in thermal conductivity enhancement. It is suggested that due to the low concentration of ND, the observed enhance of the thermal conductivity is due to the interactions (collisions) between oil molecules and NDs. At higher ND filler fraction, a percolative-like enhancement of the thermal conductivity of the solution due to the direct heat transport via collisions between ND particles can be triggered. Consequently, it was assume that the thermal conductivity constant K obey an Arrhenius like temperature dependence

$$K = K_0 \exp\left(\frac{E_A'}{K_B T}\right) \quad (11)$$

where K_0 is a constant. The Arrhenius like dependence (eq 11) fits successfully the temperature dependence of the thermal conduction coefficients.

Figure 10 shows the dependence of the activation energy E_A and pre-exponential factor K_0 on the weight fraction of NDs. It

dx.doi.org/10.1021/am405575t | ACS Appl. Mater. Interfaces 2014, 6, 4778−4785

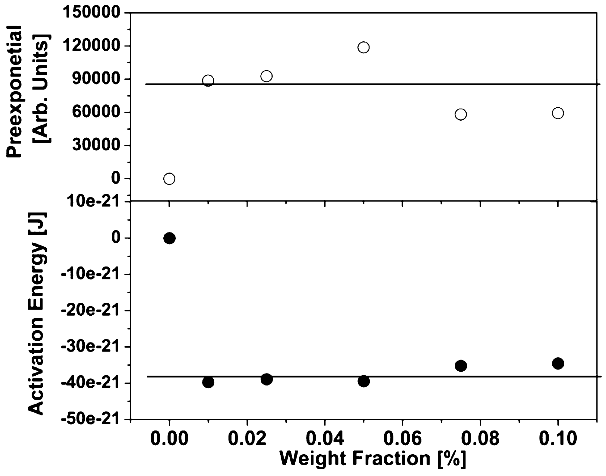

Figure 10. Dependence of the activation energy E_A' and pre-exponential factor K_0 on the weight fraction of nanodiamonds.

is noticed that the addition of nanodiamonds affected dramatically the activation energy (by about 3 orders of magnitude) as well as the pre-exponential parameter. However, in the very dilute concentration range, the dependence of both activation energy and pre-exponential factor is almost independent on the volume fraction of nanoparticles.

In conclusion, the activation energy E_A' has a sudden drop as the ND particles are added to MO and it is almost concentration independent in the dilute regime investigated in this manuscript. A similar behavior (jump), this time to higher values, was noticed in the dependence of the pre-exponential factor K_0, on the volume fraction of NDs. This suggests a percolative like transfer of heat via collisions between oil molecules and ND nanoparticles, with a very low percolation threshold. This suggests that in such a dilute regime the thermal conductivity is almost independent on the concentration of the filler while the viscosity can be controlled by controlling the concentration of NDs. This behavior can be exploited in applications that are aiming at thermal management, as viscoelastic properties can be modified without an important modification in the heat transfer properties in the limit of very dilute suspensions.

4. SUMMARY

Nanodiamond/Mineral Oil based nanofluid was investigated for potential thermal management. The study aimed at the understanding of viscoelastic and thermal properties in the dilute concentration limit, where the concentration of ND is below 0.100 wt %. It was determined that for this range of concentrations, the ND/MO dispersions behave like Newtonian fluids. However, the dependence of the dynamic viscosity on the weight fraction of filler showed that the presence of the filler affects the viscosity of the system. It was concluded from the experimental data that the effect of the volume fraction of ND on the viscosity of ND/MO solutions is well described by the Einstein theory of the viscosity (for spherical fillers). Within this simplified model, there are no interactions involving the spherical filler. The detailed study of the temperature dependence of the dynamical viscosity revealed the role of the volume fraction of nanoparticles through the dependence of the activation energy and pre-exponential factor on the volume fraction of filler. These changes are consistent with interactions involving ND nanoparticles. The role of interactions between the ND nanoparticles and MO is better observed by inspecting the dependence of the activation energy for the thermal conductivity (and of the pre-exponential factor) of the dispersions as a function of the volume fraction of ND. A potential new mechanism, similar to the percolation process and assigned to ND-MO collisions, occurring at very low weight fraction is suggested by the experimental data. At higher temperatures (>323 K) the thermal conductivity of ND-based fluids increases up to ~40 and ~70%, compared to base fluid, at 323 and 373 K, respectively; indicating the role of Brownian motion and of the ND-MO collisions, in accordance with Maxwell predictions. But many other factors such as fluids composition, viscosity, nature of base fluid (morphology as well as interaction between fluid and nanofillers), particle/fluid molecules interface, can also contribute to the enhancement in thermal conductivity of fluids.

■ AUTHOR INFORMATION

Corresponding Author

*E-mail: jtaha@ricealumni.net or jaime_taha@hotmail.com. Tel.: +1 832-248-7166. Fax: +1 713-348-5423.

Notes

The authors declare no competing financial interest.

■ ACKNOWLEDGMENTS

J.T.-T. acknowledges the support from CONACYT (213780). P.A., T.N., and J.T.-T. acknowledge funding from the Army Research Office through MURI program on novel free-Standing 2D crystalline materials focusing on atomic layers of nitrides, oxides, and sulfides (Award Number W911NF-11-1-0362). C.S.T. thanks Indian Institute of Science, Bangalore for their support.

■ REFERENCES

(1) Taha-Tijerina, J.; Narayanan, T. N.; Gao, G.; Rohde, M.; Tsentalovich, D. A.; Pasquali, M.; Ajayan, P. M. Electrically Insulating Thermal Nano-Oils Using 2D Fillers. *ACS Nano* **2012**, *6*, 1214−1220.

(2) Eastman, J. A.; Choi, S. U. S.; Li, S.; Yu, W.; Thompson, L. J. Anomalously Increased Effective Thermal Conductivities of Ethylene Glycol-Based Nanofluids Containing Copper Nanoparticles. *Appl. Phys. Lett.* **2001**, *78*, 718−720.

(3) Choi, C.; Yoo, H. S.; Oh, J. M. Preparation and Heat Transfer Properties of Nanoparticle-in-Transformer Oil Dispersions as Advanced Energy-Efficient Coolants. *Curr. Appl. Phys.* **2008**, *8*, 710−712.

(4) Xie, H.; Chen, L. Review on the Preparation and Thermal Performances of Carbon Nanotube Contained Nanofluids. *J. Chem. Eng. Data* **2011**, *56*, 1030−1041.

(5) Baby, T. T.; Sundara, R. Synthesis and Transport Properties of Metal Oxide Decorated Graphene Dispersed Nanofluids. *J. Phys. Chem. C* **2011**, *115*, 8527−8533.

(6) Gao, J. W.; Zheng, R. T.; Ohtani, H.; Zhu, D. S.; Chen, G. Experimental Investigation of Heat Conduction Mechanisms in Nanofluids. Clue on Clustering. *Nano Lett.* **2009**, *9*, 4128−4132.

(7) Zhi, C.; Xu, Y.; Bando, Y.; Golberg, D. Highly Thermo-Conductive Fluid with Boron Nitride Nanofillers. *ACS Nano* **2011**, *5*, 6571−6577.

(8) Botha, S. S.; Ndungu, P.; Bladergroen, B. J. Physicochemical Properties of Oil-Based Nanofluids Containing Hybrid Structures of Silver Nanoparticles Supported on Silica. *Ind. Eng. Chem. Res.* **2011**, *50*, 3071−3077.

(9) Lee, J.; Mudawar, I. Assessment of the Effectiveness of Nanofluids For Single-Phase and Two-Phase Heat Transfer in Micro-Channels. *Int. J. Heat Mass Transfer* **2007**, *50*, 452−463.

(10) Perry, R. H.; Green, D. W. *Perry's Chemical Engineers' Handbook*, 8th ed.; McGraw-Hill: New York, 2007.
(11) Krishnamurthy, S.; Bhattacharya, P.; Phelan, P. E.; Prasher, R. S. Enhanced Mass Transport in Nanofluids. *Nano Lett.* **2006**, *6*, 419−423.
(12) Shima, P. D.; Philip, J.; Raj, B. Synthesis of Aqueous and Nonaqueous Iron Oxide Nanofluids and Study of Temperature Dependence on Thermal Conductivity and Viscosity. *J. Phys. Chem. C* **2010**, *114*, 18825−18883.
(13) Keblinski, P.; Phillpot, S.; Choi, S. U.S .; Eastman, J. Mechanisms of Heat Flow in Suspensions of Nano-Sized Particles (Nanofluids). *Int. J. Heat Mass Transfer* **2002**, *45*, 855−863.
(14) Wen, D.; Lin, G.; Vafaei, S.; Zhang, K. Review of Nanofluids for Heat Transfer Applications. *Particuology* **2009**, *7*, 141−150.
(15) Balandin, A. A. Thermal Properties of Graphene and Nanostructured Carbon Materials. *Nat. Mater.* **2011**, *10*, 569−581.
(16) Taha-Tijerina, J.; Peña-Paras, L.; Narayanan, T. N.; Garza, L.; Lapray, C.; Gonzalez, J.; Palacios, E.; Molina, D.; García, A.; Maldonado, D.; Ajayan, P. M. Multifunctional Nanofluids With 2D Nanosheets for Thermal and Tribological Management. *Wear* **2013**, *302*, 1241−1248.
(17) Mochalin, V. N.; Shenderova, O.; Ho, D.; Gogotsi, Y. The Properties and Applications of Nanodiamonds. *Nat. Nanotechnol.* **2012**, *7*, 11−23.
(18) Yu, W.; Xie, H.; Li, Y.; Chen, L.; Wang, Q. Experimental Investigation on the Thermal Transport Properties of Ethylene Glycol Based Nanofluids Containing Low Volume Concentration Diamond Nanoparticles. *Colloids Surf., A* **2011**, *380*, 1−5.
(19) Yeganeh, M.; Shahtahmasebi, N.; Kompany, A.; Goharshadi, E. K.; Youssefi, A.; Šiller, L. Volume Fraction and Temperature Variations of the Effective Thermal Conductivity of Nanodiamond Fluids in Deionized Water. *Int. J. Heat Mass Transfer.* **2010**, *53*, 3186−3192.
(20) Shenderova, O.; Tyler, T.; Cunningham, G.; Ray, M.; Walsh, J.; Casulli, M.; Hens, S.; McGuire, G.; Kuznetsov, V.; Lipa, S. Nanodiamond and Onion-Like Carbon Polymer Nanocomposites. *Diamond Relat. Mater.* **2007**, *16* (4−7), 1213−1217.
(21) Ozawa, M.; Inaguma, M.; Takahashi, M.; Kataoka, F.; Krüger, A.; Ōsawa, E. Preparation and Behavior of Brownish, Clear Nanodiamond Colloids. *Adv. Mater.* **2007**, *19*, 1201−1206.
(22) Branson, B. T.; Beauchamp, P. S.; Beam, J. C.; Lukehart, C. M.; Davidson, J. L. Nanodiamond Nanofluids for Enhanced Thermal Conductivity. *ACS Nano* **2013**, *7*, 3183−3189.
(23) Behler, K. D.; Stravato, A.; Mochalin, V.; Korneva, G.; Yushin, G.; Gogotsi, Y. Nanodiamond-Polymer Composite Fibers and Coatings. *ACS Nano* **2009**, *3*, 363−369.
(24) Speight, J. G. *Lange's Handbook of Chemistry*, 16th ed.; McGraw-Hill: New York, 2004.
(25) Yamamoto, Y.; Imai, T.; Tanabe, K.; Tsuno, T.; Kumazawa, Y.; Fujimori, N. The Measurement of Thermal Properties of Diamond. *Diamond Relat. Mater.* **1997**, *6*, 1057−1061.
(26) Wei, L.; Kuo, P. K.; Thomas, R. L.; Anthony, T. R.; Banholzer, W. F. Thermal Conductivity of Isotopically Modified Single Crystal Diamond. *Phys. Rev. Lett.* **1993**, *70*, 3764−3767.
(27) Kang, H. U.; Kim, S. H.; Oh, J. M. Estimation of Thermal Conductivity of Nanofluid Using Experimental Effective Particle Volume. *Exp. Heat Transfer* **2006**, *19*, 181−191.
(28) Chen, L.; Xie, H. Silicon Oil Based Multiwalled Carbon Nanotubes Nanofluid With Optimized Thermal Conductivity Enhancement. *Colloids Surf., A* **2009**, *352*, 136−140.
(29) Yu, W.; Xie, H.; Bao, D. Enhanced Thermal Conductivities of Nanofluids Containing Graphene Oxide Nanosheets. *Nanotechnology* **2010**, *21*, 055705.
(30) Wang, X.; Xu, X.; Choi, S. U. S. Thermal Conductivity of Nanoparticle - Fluid Mixture. *J. Thermophys. Heat Transfer* **1999**, *13*, 474−480.
(31) Liu, M.-S.; Ching-Cheng Lin, M.; Huang, I.-T.; Wang, C.-C. Enhancement of Thermal Conductivity With Carbon Nanotube for Nanofluids. *Int. Commun. Heat Mass Transfer* **2005**, *32*, 1202−1210.
(32) Williams, O. A.; Hees, J.; Dieker, C.; Jäger, W.; Kirste, L.; Nebel, C. E. Size-Dependent Reactivity of Diamond Nanoparticles. *ACS Nano* **2010**, *4*, 4824−4830.
(33) Chipara, D. M.; Chipara, A. C.; Chipara, M. Raman Spectroscopy of Carbonaceous Materials: A Concise Review. *Spectroscopy* **2011**, *26*, 42−47.
(34) Filik, J.; Harvey, J. N.; Allan, N. L.; May, P. W.; Dahl, J. E. P.; Liu, S.; Carlson, R. M. K. Raman Spectroscopy of Nanocrystalline Diamond: An *ab initio* Approach. *Phys. Rev. B* **2006**, *74*, 035423.
(35) Ferrari, A. C.; Robertson, J. Raman Spectroscopy of Amorphous, Nanostructured, Diamond−Like Carbon, and Nanodiamond. *Philos. Trans. R. Soc. London, A* **2004**, *362*, 2477−2512.
(36) Tiwary, C. S.; Kumbhakar, P.; Mitra, A. K.; Chattopadhyay, K. Synthesis of Wurtzite-Phase ZnS Nanocrystal and Its Optical Properties. *J. Lumin.* **2009**, *129*, 1366−1370.
(37) Choi, S. U. S. Nanofluids: From Vision to Reality Through Research. *J. Heat Transfer* **2009**, *131*, 033106-1−033106-9.
(38) Jeffrey, D. J.; Acrivos, A. The Rheological Properties of Suspensions of Rigid Particles. *AIChE J.* **1976**, *22*, 417−432.
(39) Mueller, S.; Llewellin, E. W.; Mader, H. M. The Rheology of Suspensions of Solid Particles. *Proc. R. Soc. London, Ser. A* **2010**, *466*, 1201−1228.